Thermodynamics and heat transport of a disordered antiferromagnet $3R$-Na_2MnTeO_6

Na Li（李娜）,[1,*] Shuang-Kui Guang（光双魁）,[2,*] Hui Liang（梁慧）,[1] Dan-Dan Wu（吴丹丹）,[1] Yan Sun（孙燕）,[1] Qiu-Ju Li（李秋菊）,[3] Zi-Yang Wu（吴紫阳）,[4] Jun-Feng Wang（王俊峰）,[4] Guan-Yin Gao（高关胤）,[5] Ying Zhou（周颖）,[1,†] Xia Zhao（赵霞）,[2,‡] and Xue-Feng Sun（孙学峰）[1,2,§]

[1] *Anhui Provincial Key Laboratory of Magnetic Functional Materials and Devices, Institutes of Physical Science and Information Technology, Anhui University, Hefei, Anhui 230601, China*
[2] *School of Physical Sciences, University of Science and Technology of China, Hefei, Anhui 230026, China*
[3] *Anhui Provincial Key Laboratory of Magnetic Functional Materials and Devices, School of Physics and Optoelectronics, Anhui University, Hefei, Anhui 230061, China*
[4] *Wuhan National High Magnetic Field Center, Huazhong University of Science and Technology, Wuhan, Hubei 430074, China*
[5] *Hefei National Laboratory for Physical Sciences at Microscale, University of Science and Technology of China, Hefei, Anhui 230026, China*

(Dated: September 29, 2026)

We study the low-temperature thermal conductivity, specific heat and magnetic susceptibility of $3R$-Na_2MnTeO_6 single crystal, which is a layered antiferromagnet. Magnetic susceptibility shows no magnetic transition at low temperatures down to 2 K, while the antiferromagnetic interaction was confirmed by the negative Curie-Weiss temperatures for both interlayer and intralayer susceptibility. Ultralow-temperature specific heat down to 80 mK also displays the absence of magnetic ordering. Whereas, the low-temperature ac susceptibility indicates spin freezing around 1 K. Ultralow-temperature thermal conductivity shows a T^2-dependence with very small magnitude, which seems to be compatible with the spin glass state. However, both the in-plane and out-of-plane magnetic fields suppress the thermal conductivity rather strongly, which is quite different from the known behavior of that in the spin glass systems. These results suggest a ground state with spin freezing rather than the canonical spin glass.

Keywords: Spin freezing, thermal conductivity
PACS: 66.25.+g, 71.27.+a, 75.50.Lk

I. INTRODUCTION

Low-dimensional magnetic systems are of great interest for the discoveries of exotic quantum phenomena, including the quantum spin liquids (QSLs) and magnetic transitions associated with the magnetization plateau etc. [1–10] For either Heisenberg-type or Ising-type spin systems, the ground state can be prevented from attaining long-range order at finite temperatures through the Mermin-Wagner theorem [11] or geometric frustration [1, 4]. Typical quantum fluctuations become significant in low-dimensional magnets with small spin number [5]. For example, in $S = 1/2$ antiferromagnets the geometric frustration can induce a QSL state [3] while systems with $S = 3/2$ or $5/2$ usually exhibit the long-range ordered ground states [12, 13]. Besides geometric frustration, non-negligible interlayer interactions and inherent structural/chemical disorder can also play vital roles in determine the low-dimensional quantum magnetisms [14–16]. Disorder is particularly consequential for QSL candidates: random site occupancy and stacking faults introduce a distribution of local exchange fields, which can localize possible itinerant spin excitations and eventually drive an inhomogeneous, glassy freezing of spins rather than a collective liquid state, as has been argued for the site-disordered triangular compounds $YbMgGaO_4$ and $YbZnGaO_4$ [17–20]. This motivates an open question: what ground state is realized in $S = 3/2$ magnets with coexisting geometric frustration and intrinsic structural disorder, among long-range magnetic order, QSL, and disorder-induced spin freezing?

A material family for examining this question is the trigonal layered quaternary tellurates trigonal layered quaternary tellurates A_2MTeO_6 (A = Li, Na and M = Ti, Mn, Sn, Ge), which contains stacked two-dimensional (2D) honeycomb layers [21, 22]. The tetravalent magnetic ions Mn^{4+} form a diluted triangular net within the layers, which were separated by the Te^{6+} ions. The overall arrangement of both Mn^{4+} and Te^{6+}, centered in the edge-sharing octahedra, form the honeycomb layers. The interlayer space in these compounds is filled by the dense package of the alkali ions centered in the face-sharing trigonal prisms. Some previous work suggested a hidden magnetic order in A_2MnTeO_6 [23]. The dc susceptibility does not show obvious development of long-range magnetic order in weak magnetic field, while a clear maximum on $\chi(T)$ was observed in sufficiently high external magnetic field, which corresponds to the onset of long-range antiferromagnetic order at low temperatures. Neutron power diffraction has revealed a 120° noncollinear spin arrangement for Li_2MnTeO_6 with the propagation vector $\boldsymbol{k}$ = (1/3, 1/3, 0) [23] and a commensurate 120° spin helix for $2H$-Na_2MnTeO_6 with propagation vector $\boldsymbol{k}$ = (1/3, 1/3, 1/3) [24], respectively. Recently, Xu *et al.*

* These authors contributed equally to this work.
† yzhou@ahu.edu.cn
‡ xiazhao@ustc.edu.cn
§ xfsun@ahu.edu.cn

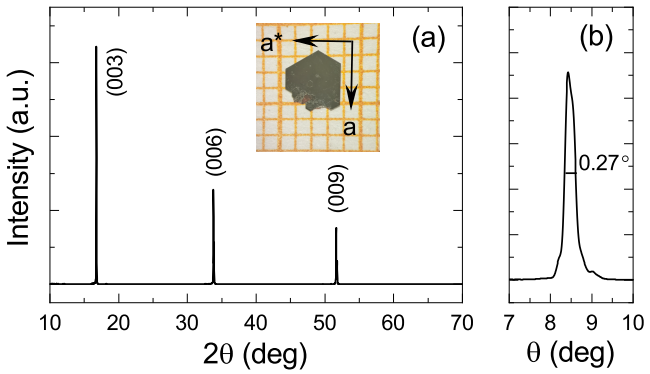


FIG. 1. X-ray diffraction pattern of (00l) plane and the rocking curve of the (003) peak. The full width at the half maximum (FWHM) of the rocking curve is shown in panel (b). The inset shows the photograph of $3R$-Na_2MnTeO_6 single crystal grown in this work.

reported the synthesis of single crystals of ABC-stacking honeycomb layered magnet $3R$-Na_2MnTeO_6 [25], which has an $R\bar{3}$ lattice and exhibits distinct magnetism from the hexagonal AB stacking compound $2H$-Na_2MnTeO_6 [24]. Their results demonstrated that $3R$-Na_2MnTeO_6 could be a good platform for studying the magnetic excitation continuum in low-dimensional systems and the interplay between intersite disorder and spin-disordered states. However, the nature of the ground state is still not identified for $3R$-Na_2MnTeO_6.

Ultralow-temperature thermal conductivity (κ) has been widely used for studying the elementary excitations in quantum magnets since it can effectively detect the itinerant excitations. The most famous example is that a finite residual linear term κ_0/T can be taken as a smoking gun for the existence of itinerant gapless spinons in QSLs [17, 26–28]. The magnetic field dependence of κ was also found to be sensitive to field-induced quantum magnetic transitions [9, 10, 28]. The advantage of thermal conductivity measurement is that it avoids the effects of localized excitations caused by the inevitable impurities in these materials [29].

In this work, we study the thermal conductivity, magnetic susceptibility and specific heat of $3R$-Na_2MnTeO_6 single crystals at very low temperatures. The magnetic susceptibility and specific heat results verified the absence of long-range order down to 80 mK, while a spin freezing occurs at about 1 K. The ultralow-temperature thermal conductivity has very small magnitude and T^2 dependence, which is compatible with the spin glass state. However, the external magnetic field gradually suppresses the κ. These results point to a ground state with spin freezing rather than the canonical spin glass.

II. EXPERIMENTS

High-quality single crystals of $3R$-Na_2MnTeO_6 were grown by a flux method [25]. The as-grown crystals are black hexagonal flakes with typical size of $\sim 3 \times 3 \times 0.1$ mm^3, as shown in the inset to Fig. 1(a), and are easily cleaved along the ab plane. The orientation of crystals was confirmed by X-ray Laue back diffraction. Figures 1(a) and 1(b) show the (00l) diffraction and the rocking curve of (003) peak, which indicate the good crystallinity of these crystals. Moreover, the energy dispersive X-ray elemental analysis indicates that the element content in our samples is in good agreement with the chemical formula. The dc magnetic susceptibility between 2 and 300 K were measured using the SQUID-VSM (Quantum Design Magnetic Property Measurement System, MPMS) in magnetic field up to 7 T. The high-field magnetization was measured in the Wuhan National High Magnetic Field Center (WHMFC). The ac susceptibility and specific heat were measured using the Physical Property Measurement System (PPMS) (DynaCool, Quantum Design) with a dilution insert. Thermal conductivity was measured by using a "one heater, two thermometers" technique in a ^{3}He/^{4}He dilution refrigerator at 70 mK – 1.2 K and in a ^{3}He refrigerator at 0.3 K – 30 K, equipped with a 14 T superconducting magnet [10, 17, 28]. The thermal Hall effect was measured by using the standard steady-state technique with "one heater, three thermometers" [30].

III. RESULTS AND DISCUSSION

A. Magnetic properties

Figures 2(a-c) present the temperature dependence of magnetic susceptibility χ measured with $B = 0.01$ T along the c, a and $a*$ (the in-plane direction perpendicular to the a axis) axis, respectively. The $\chi(T)$ increases upon lowering temperature and there is no visible anomaly down to 2 K, indicating the absence of long-range magnetic order. It should be pointed out that there is also no clear maximum or sharp peak in $\chi(T)$ curves with 7 T magnetic field along any crystallographic axis (not shown in the figures), which precludes the hidden long-range magnetic order [23]. The Curie-Weiss fit to the low-temperature data (2 – 50 K) gives effective moment $\mu_{eff} = 3.94\ \mu_B$, Curie-Weiss temperature $\theta_{CW} = -5.503$ K for $B \parallel c$ and $\mu_{eff} = 3.24\ \mu_B$, $\theta_{CW} = -5.066$ K for $B \parallel a$, $\mu_{eff} = 3.26\ \mu_B$, $\theta_{CW} = -5.113$ K for $B \parallel a*$, respectively. The negative θ_{CW} indicates the dominant interlayer and intralayer antiferromagnetic interactions. The field-cooling (FC) and zero-field-cooling (ZFC) susceptibility data does not show detectable difference, ruling out the possibilities of ferromagnetic moments or spin freezing down to 2 K. Figures 2(d-f) show the isothermal magnetization curves at 2, 5 and 10 K with the external magnetic fields along the c, a, and $a*$ axis, respectively. The $M(B)$ curves exhibit weak anisotropy and no field-induced transitions under the external fields up to 7 T for all three directions. These results are in good agreement with the previous report [25]. Figure 3 shows the

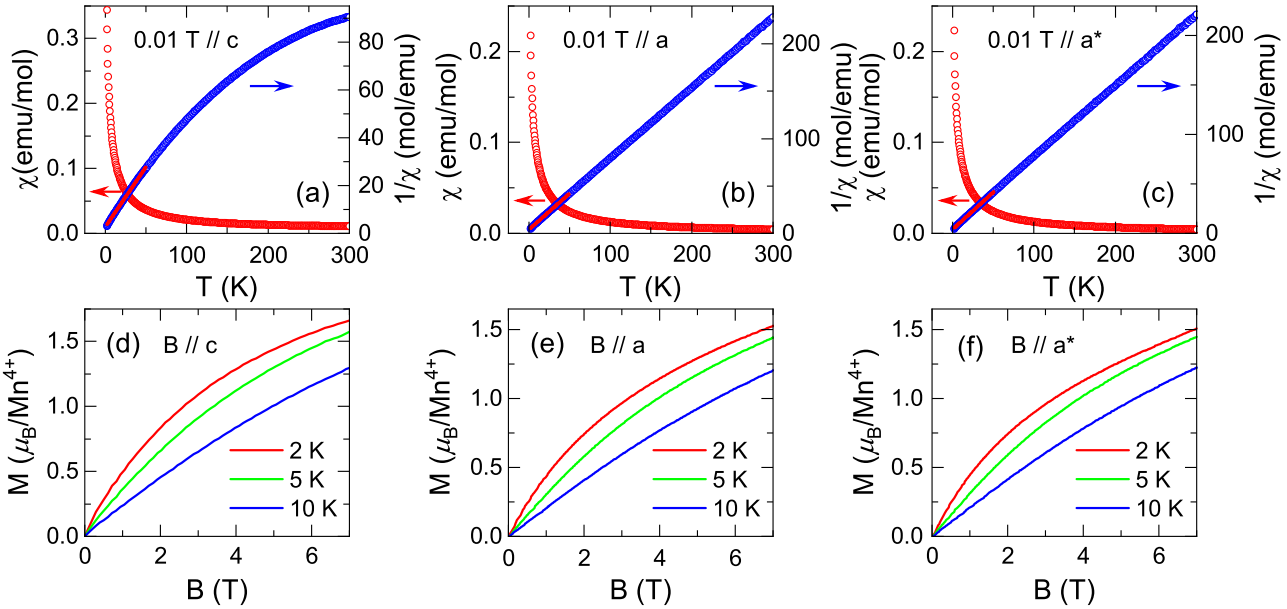


FIG. 2. (a-c) Temperature dependence of magnetic susceptibility χ and inverse magnetic susceptibility $1/\chi$ of Na_2MnTeO_6 single crystal with $B \parallel c$, $B \parallel a$ and $B \parallel a*$. The solid red lines indicate the linear fit of the inverse magnetic susceptibility $1/\chi(T)$ curves. (d-f) Isothermal magnetization at selected temperatures with $B \parallel c$, $B \parallel a$ and $B \parallel a*$.

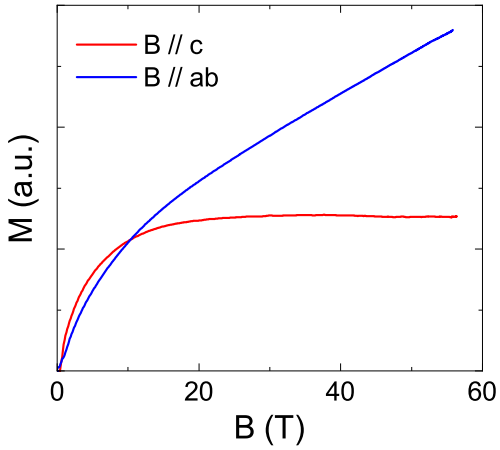


FIG. 3. High-field magnetization curves of $3R$-Na_2MnTeO_6 single crystals at 2 K with the external magnetic fields along the c axis or the ab plane.

high-field magnetization curves for magnetic field along the c axis or the ab plane, which do not exhibit any clear anomaly. The c-axis magnetization was saturated around 20 T with the saturation moment of $2.4\mu_B/Mn^{4+}$, while the in-plane magnetization was not at fields up to 56 T.

The previous work reported that the ac susceptibility of $3R$-Na_2MnTeO_6 single crystal shows no anomaly or frequency dependence down to 1.8 K [25]. To further characterize the magnetic ground state of $3R$-Na_2MnTeO_6, we measured the ac susceptibility at very low temperatures down to 100 mK. Figure 4(a) shows the temperature dependence of the real part χ' measured in the absence of dc field. Clearly, there is a frequency-dependent peak around 1.3–1.6 K, which indicates spin freezing. One can analyze this frequency dependence to clarify whether it is a spin glass state. A phenomenological classification can be done by estimating the Mydosh parameter $\delta = \Delta T_f/(T_f \Delta \log f)$ [31, 32], where T_f is the freezing temperature defined as the peak position in $\chi'(T)$. This is a quantitative measure of the relative peak shift of χ' with frequency and usually used as a criterion to distinguish the conventional spin glass, cluster glass, and superparamagnetic systems. For $3R$-Na_2MnTeO_6, δ is calculated to be 0.094, as shown in Fig. 4(b). This value is rather different to that of the canonical spin-glass systems ($\delta \sim 0.005$) [31, 32]. We note a similar case for the famous quantum spin-ice material $Tb_2Ti_2O_7$, in which the frequency dependence of the ac susceptibility does not correspond to a canonical spin-glass transition but rather to a spin freezing [33]. The δ of $Tb_2Ti_2O_7$ was found to be 0.06–0.08, which is comparable to that of $3R$-Na_2MnTeO_6. Well-established literature benchmarks are: the Mydosh parameter $\delta = 0.005 - 0.01$ for canonical spin glasses, $\delta = 0.01 - 0.08$ for cluster glasses, and $\delta > 0.1$ for non-interacting superparamagnets. In our work, the Mydosh parameter $\delta \sim 0.094$ lies at the upper end of the cluster-glass range, close to the superparamagnetic limit, and is substantially larger than the benchmark value for canonical spin glasses. Moreover, the weak frequency dependence indicates that the freezing may originate from short-range correlated magnetic clusters, i.e., cluster-glass-type inhomogeneous moment freezing induced by structural disorder, rather than from the thermodynamic spin-glass transition of a canonical

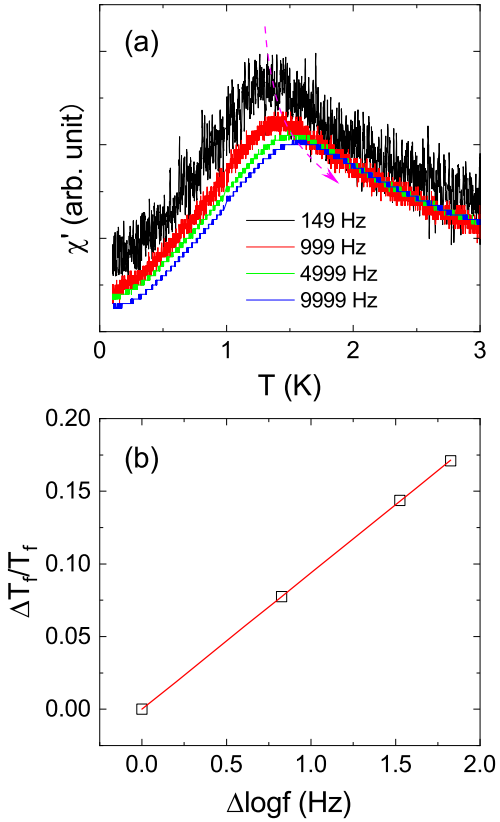


FIG. 4. (a) Temperature dependencies of the ac magnetic susceptibility measured in zero dc field with different frequencies. The ac field is applied along the c axis. The dashed arrow is the guide to eyes for the peak position. (b) Frequency dependence of the freezing temperature plotted as $\Delta T_f/T_f$ versus $\Delta \log f$. The slope of the fitted straight line is the Mydosh parameter δ.

spin glass.

B. Specific heat

Figure 5(a) shows the zero-field specific heat of $3R$-Na_2MnTeO_6 single crystal. Clearly, there is no phase transition at low temperatures down to 80 mK, which indicates the disordered ground state of this material. In the previous report, the specific heat data also indicated the absence of magnetic order at low temperatures down to 0.5 K [25]. It is notable that there is a broad hump at temperatures around 8 K and the broad hump shifts toward higher temperatures with increasing magnetic field and develops into a kink at 9 T, as shown in Fig. 5(c), which might suggest the short-range spin correlations. At very low temperatures, the upturn feature is likely due to the nuclear Schottky contribution of Mn^{4+} ions. With applying magnetic field along the c axis, both the nuclear Schottky anomaly and the short-range hump are obviously affected, which is easily to understand. Nevertheless, our ultralow-temperature specific heat data confirm the absence of long-range order in $3R$-Na_2MnTeO_6, which is distinct from the analog compounds $2H$-Na_2MnTeO_6 [24] and Li_2MnTeO_6 [23], in which the zero-field specific heat displays a distinct λ-type anomaly.

The phonon specific heat is dominant at high-temperature regime. We found that the high-temperature specific heat data can be fitted by the formula considering both the Debye and Einstein models [10, 34–36], that is,

$$\begin{aligned} C_{\rm ph} = {} & 3N_D R\left(\frac{T}{\Theta_D}\right)^3 \int_0^{\Theta_D/T} \frac{x^4 e^x}{(e^x-1)^2}\mathrm{d}x \\ & + N_{E1} R\left(\Theta_{E1}/T\right)^2 \frac{\exp(\Theta_{E1}/T)}{[\exp(\Theta_{E1}/T)-1]^2} \\ & + N_{E2} R\left(\Theta_{E2}/T\right)^2 \frac{\exp(\Theta_{E2}/T)}{[\exp(\Theta_{E2}/T)-1]^2} \\ & + N_{E3} R\left(\Theta_{E3}/T\right)^2 \frac{\exp(\Theta_{E3}/T)}{[\exp(\Theta_{E3}/T)-1]^2}, \end{aligned} \tag{1}$$

with $x = \hbar\omega/k_B T$, ω the phonon frequency, k_B the Boltzmann constant, and R the universal gas constant. In the above formula, the first term is the contribution of 3 acoustic phonon branches described by the Debye model ($N_D = 3$), while the other terms are the contributions from the optical branches described by the Einstein model ($N_{E1} = 6$, $N_{E2} = 9$ and $N_{E3} = 12$). Other parameters are the Debye temperature, $\Theta_D = 197$ K, and three Einstein temperatures, $\Theta_{E1} = 309$ K, $\Theta_{E2} = 657$ K and $\Theta_{E3} = 1489$ K.

At very low temperatures, the phonon specific heat calculated from the above formula is negligibly small, as shown by the red line in Fig. 5(b). Moreover, the nuclear hyperfine contribution C_{hyp} can be adequately represented by α/T^2 at lowest temperature and we fitted the data with this expression demonstrates that the nuclear hyperfine contribution is negligible between 0.5 and 1 K. Therefore, the very-low-temperature specific heat is dominated by the magnetic and nuclear contributions. In zero field, the magnetic specific heat displays a T-linear behavior at $T < 1$ K, which is a typical result for spin glass [37, 38]. With increasing magnetic field, the magnetic specific heat is gradually decreased. This is compatible with the suppression of magnetic excitations in spin glass by the external magnetic field [39, 40].

C. Thermal conductivity

Figure 6(a) shows the thermal conductivity of Na_2MnTeO_6 single crystal in zero field and 14 T field along the c or $a*$ axis, respectively. There are several notable features of the zero-field data. First, the $\kappa(T)$ curve does not display any anomaly at 70 mK – 30 K, which is consistent with the specific heat data regarding to the absence of magnetic phase transition. Second, the magnitudes of κ are very small in the whole temperature range, compared to other single crystal samples of insulator. Even the common phonon peak, usually appearing

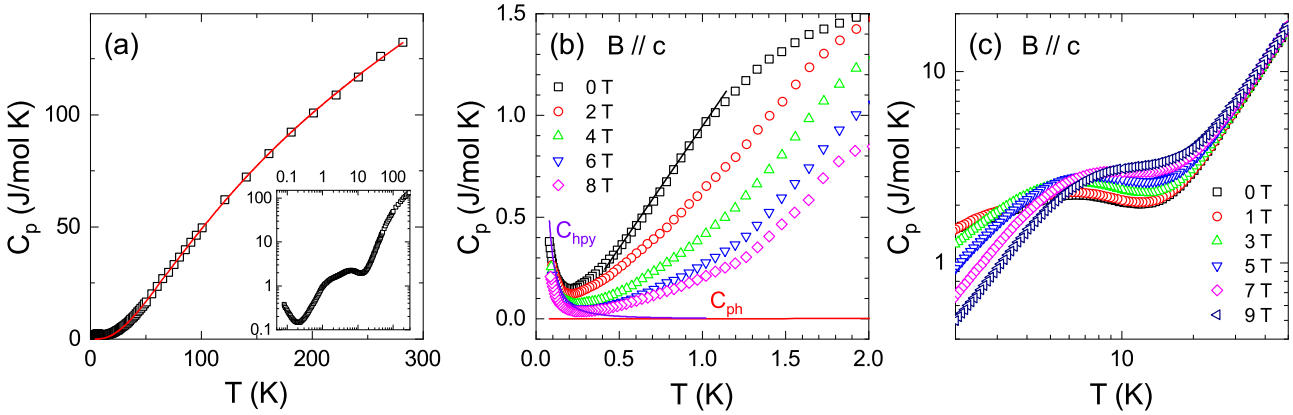


FIG. 5. (a) Specific heat of $3R$-Na_2MnTeO_6 single crystal in zero field and at 80 mK – 300 K. The inset shows the log-log plot of the data. (b) Ultralow-temperature specific heat in zero field and various magnetic fields applied along the c axis. The red line is the fitting result of high-temperature phononic specific heat. The purple line represents the contribution from the nuclear hyperfine. The black line indicates the linear behavior of specific heat at $T < 1$ K. (c) The temperature dependencies of $C_p(T)$ taken at various magnetic fields applied along the c axis.

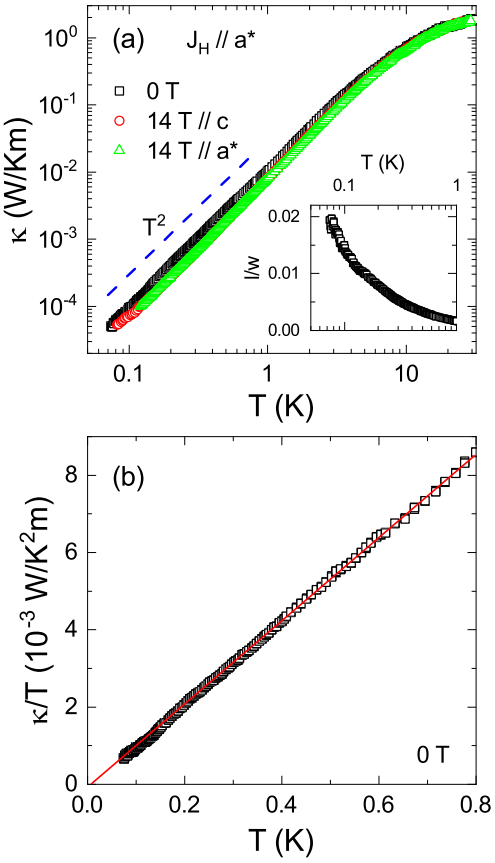


FIG. 6. (a) Zero-field thermal conductivity of $3R$-Na_2MnTeO_6 single crystal in temperature range of 70 mK – 30 K. The heat current is along the $a*$ axis (perpendicular to a axis). Also shown are the thermal conductivity in 14 T magnetic field along the c or the $a*$ axis. The inset shows the temperature dependence of the phonon mean free path l divided by the averaged sample width W. (b) Data in zero field plotted in κ/T vs T. The solid line is a linear fit of the data.

at 10 – 20 K, does not show up in these data. This also points to the extremely weak phonon thermal conductivity. Third, the low temperature κ exhibits a T^2 behavior, which strongly deviates from the standard T^3 behavior of phonon thermal conductivity [41].

Such small thermal conductivity seems to suggest that there is no other kind of heat carriers than phonons. Assuming that the thermal conductivity is purely phononic at low temperatures, the phonon mean free path can be calculated [42]. The phononic thermal conductivity can be expressed by the kinetic formula $\kappa_{ph} = \frac{1}{3}Cv_pl$ [41], where $C = \beta T^3$ is the phonon specific heat at low temperatures, v_p is the average velocity and l is the mean free path of phonon. The β and v_p can be obtained from Debye temperature using the relations $\beta = \frac{12\pi^4}{5}\frac{Rs}{\Theta_D^3}$ and $\Theta_D = \frac{\hbar v_p}{k_B}(\frac{6\pi^2 Ns}{V})^{\frac{1}{3}}$ [43], where N is the number of molecules per mole and each molecule comprises s atoms, V is the volume of crystal and R is the universal gas constant. With the above Debye temperature from the specific heat data, we obtained $\beta = 2.54\times10^{-3}$ J/K^{4}mol and $v_p = 1510$ m/s. The inset to Fig. 6(a) shows the ratio of calculated l to the averaged sample width $W = 2\sqrt{A/\pi}$ = 0.367 mm [41, 44], where A is the area of cross section. It can be seen that although the l/W increases with lowering temperature, it is still smaller than 0.02 ($\ll 1$) at the lowest temperature, which means that the boundary scattering limit is far from being established at such low temperatures. It should be noted that the phonon mean free path would be over-estimated if there were sizeable contribution to κ from other heat carriers. Nevertheless, the very small κ demonstrates that the phonon heat transport in $3R$-Na_2MnTeO_6 single crystal is actually a very special case.

Figure 6(a) also show that when applying 14 T magnetic field along either the c or $a*$ axis, the κ are clearly decreased, with nearly T^2 dependence at very low tem-

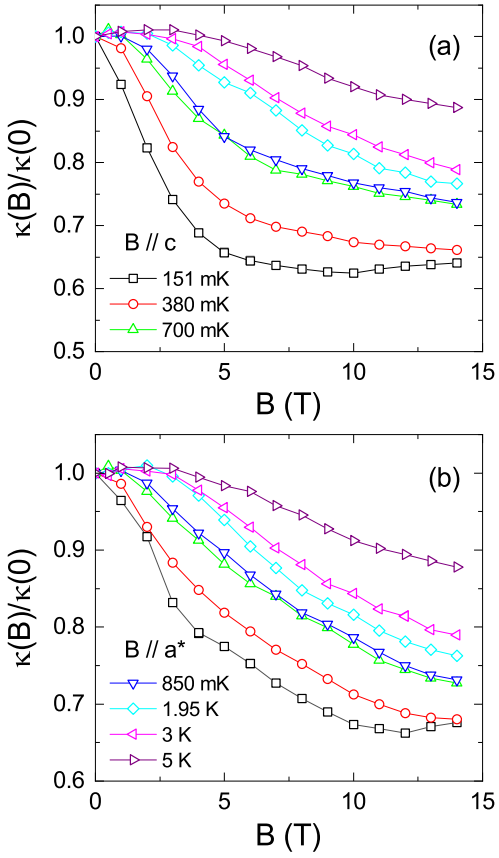


FIG. 7. Magnetic field dependence of thermal conductivity at different temperatures with magnetic field along the c (a) and the $a*$ (b) directions.

peratures. This may indicate the enhanced magnetic scattering of phonons induced by magnetic field. Another possible reason for the suppression of κ in such high field is that there might be some magnetic excitations transporting heat in zero field, which is suppressed by magnetic field. Many previous studies on QSL candidates revealed that at very low temperatures the thermal conductivity usually can be fitted to $\kappa/T = \kappa_0 + bT^{\alpha-1}$, in which the two terms represent contributions from the itinerant fermionic magnetic excitations and phonons, respectively [17, 26–28]. To check this possibility, Fig. 6(b) shows the ultralow-temperature data at zero field plotted with κ/T vs T. It is clear that the linear fitting actually gives $\kappa_0/T = 0$, which excludes the possibility of the existence of itinerant fermionic magnetic excitations at zero field. It should be pointed out that the zero κ_0/T does not necessarily suggest the absence of spinons or QSL, since in some QSL candidates like $PrMgAl_{11}O_{19}$, $NaYbS_2$ and $NaYbSe_2$, the strong spinon-phonon scattering could yield zero κ_0/T [49, 51]. However, in these materials the ultralow-temperature κ is enhanced in strong magnetic fields that can polarize the spins.

Figure 7 shows the field dependence of the thermal conductivity with magnetic field along the c axis or $a*$ axis, which display nearly isotropic magneto-thermal effect for these two field directions. It can be seen that at the lowest temperature of 151 mK, the field-suppression effect is the most significant and it becomes weaker with increasing temperature. Moreover, there is no sharp anomaly in the $\kappa(B)$ curves, which indicates that there is no field-induced magnetic transitions [10, 52–54]. This is consistent with the above magnetization results. Here, the almost monotonic decrease of the κ with field is very difficult to understand. First, it should be pointed out the magnetic field dependence of κ can sometimes result from the resonant scattering by the free spins [55–57]. The paramagnetic resonant phonon scattering is most effective in suppressing the phonon transport when the energy splitting with Zeeman effect is equal to $\sim 3.8k_BT$, where the phonon conductivity spectrum peaks [41]. Therefore, the spin-phonon scattering generates a dip-like feature in $\kappa(B)$ and the dip position shifts to higher field with increasing temperature. In the high-field limit, the spin energy splitting is too large for spins to exchange energy with phonons and the spin-phonon scattering is quenched; as a result, the high-field κ will recover the zero-field value. However, for $3R$-Na_2MnTeO_6 at least the 14 T field along the c axis still strongly suppresses the κ, while this field nearly polarizes the spins (see the high-field magnetization curve in Fig. 3). In addition, the specific heat data do not show the existence of free spins, which would give Schottky contribution with a broad-peak feature shifting upon increasing magnetic field. Apparently, the $\kappa(B)$ behavior of $3R$-Na_2MnTeO_6 cannot be ascribed to the resonant phonon scattering by the free spins. Second, if there were spinon excitations that strongly scatter with phonons, applying magnetic field would suppress the magnetic excitations and weaken the scattering; thus one would expect the enhancement of κ in strong magnetic fields [17, 48, 49, 51], which however is opposite to the experimental results. Moreover, Our $\kappa(B)$ data show a monotonic reduction upon increasing magnetic field without any signature of a field-induced transition. This behavior differs remarkably from the $\kappa(B)$ behaviors reported for those QSL candidates, α-$RuCl_3$, $Na_2BaCo(PO_4)_2$, $YbMgGaO_4$, and $NaYbSe_2$ [17, 28, 51, 58]. These materials have several different $\kappa(B)$ features: (i) there is non-monotonic magnetic field dependence of thermal conductivity; (ii) there are clear anomalies in $\kappa(B)$ that are related to some field-induced magnetic transition; (iii) the $\kappa(B)$ are enhanced and saturated in enough high fields. For this reason, the present $\kappa(B)$ behaviors are not compatible with those of QSL candidates. Third, the phonon thermal conductivity in the spin-glass materials was found to be enhanced in magnetic fields [59, 60]. It is known that the low-temperature behavior of spin glasses can be described in terms of magnetic two-level systems [59, 60], which are associated with regions of complex spin arrangements (spin clusters) whose spin rotations are blocked by the anisotropy energy barriers. The magnetic two-level systems can be activated over their energy barriers by in-

elastic scattering of phonons, coupled via the spin-orbital interaction. Thus, the low-temperature phonon thermal conductivity of spin glasses usually has weak temperature dependence (T^2) and small magnitude. Applying magnetic field would block the spin clusters and the magnetic excitations are prohibited. This natively explained the common field-induced enhancement of thermal conductivity. This magnetic field dependence of κ is quite different from the present result of $3R$-Na_2MnTeO_6. Therefore, the low-temperature thermal conductivity of $3R$-Na_2MnTeO_6 exhibits rather unusual properties and is incompatible with that of canonical spin glass.

In passing, we measured the thermal Hall effect of $3R$-Na_2MnTeO_6 single crystals at low temperatures. It was found that at 0.7 – 5 K there is no sizable thermal Hall signal, which also rules out the possible transport of magnetic excitations.

To summarize the present experimental results, $3R$-Na_2MnTeO_6 has a spin disordered ground state. Furthermore, the ac susceptibility suggest a spin-freezing rather than spin-glass state, which is somewhat similar to the well-known pyrochlore $Tb_2Ti_2O_7$ [33]. The temperature dependence of κ ($\sim T^2$) is compatible with that of spin-glass materials, while the magnetic field dependence of κ is distinctly different from that of spin glass. Further theoretical investigations are called for to understand the nature of ground state and unusual heat transport properties of this interesting material.

IV. CONCLUSION

We study the low-temperature thermal conductivity, specific heat and magnetic susceptibility of layered antiferromagnet $3R$-Na_2MnTeO_6. No magnetic order was probed by the magnetic susceptibility and specific heat data at low temperatures down to 80 mK, while a spin freezing was detected at about 1 K. Ultralow-temperature thermal conductivity shows a T^2-dependence with very small magnitude, which is compatible with the spin glass state. However, the magnetic field dependence of thermal conductivity is quite different from the usual behavior of that in spin glass systems. Based on the ac susceptibility and thermal conductivity results, this material has a spin-freezing rather than spin-glass ground state.

ACKNOWLEDGMENTS

This work was supported by the National Key Research and Development Program of China (Grant No. 2023YFA1406500), the National Natural Science Foundation of China (Grant Nos. 12404043, 12174361, 12274388, and 12574042) and the Nature Science Foundation of Anhui Province (Grant No. 2408085QA024).

[1] Balents L 2010 *Nature (London)* **464** 199
[2] Zhou Y, Kanoda K, and Ng T-K 2017 *Rev. Mod. Phys.* **89** 025003
[3] Savary L and Balents L 2017 *Rep. Prog. Phys.* **80** 016502
[4] Broholm C, Cava R J, Kivelson S A, Nocera D G, Norman M R and Senthil T 2020 *Science* **367** eaay0668
[5] Vasiliev A, Volkova O, Zvereva E and Markina M 2018 *npj Quantum Mater.* **3** 18
[6] Shirata Y, Tanaka H, Matsuo A and Kindo K 2012 *Phys. Rev. Lett.* **108** 057205
[7] Susuki T, Kurita N, Tanaka T, Nojiri H, Matsuo A, Kindo K and Tanaka H 2013 *Phys. Rev. Lett.* **110** 267201
[8] Zhou H D, Xu C, Hallas A M, Silverstein H J, Wiebe C R, Umegaki I, Yan J Q, Murphy T P, Park J H, Qiu Y, Copley J R D, Garder J S and Takano Y 2012 *Phys. Rev. Lett.* **109** 267206
[9] Fortune N A, Huang Q, Hong T, Ma J, Choi E S, Hannahs S T, Zhao Z Y, Sun X F, Takano Y and Zhou H D 2021 *Phys. Rev. B* **103** 184425
[10] Li N, Huang Q, Brassington A, Yue X Y, Chu W J, Guang S K, Zhou X H, Gao P, Feng E X, Cao H B, Choi E S, Sun Y, Li Q J, Zhao X, Zhou H D and Sun X F 2021 *Phys. Rev. B* **104** 104403
[11] Mermin N D and Wagner H 1966 *Phys. Rev. Lett.* **17** 1133
[12] Seki S, Onose Y and Tokura Y 2007 *Phys. Rev. Lett.* **101** 067204
[13] Svistov L E, Smirnov A I, Prozorova L A, Petrenko O A, Micheler A, Büttgen N, Shapiro A Ya and Demianets L N 2006 *Phys. Rev. B* **74** 024412
[14] Furakawa T, Miyagawa K, Itou T, Ito M, Taniguchi H, Saito M, Iguchi S, Sasaki T and Kanoda K 2015 *Phys. Rev. Lett.* **115** 077011
[15] Zhong R, Chung M, Kong T, Nguyen L T, Lei S and Cava R J 2018 *Phys. Rev. B* **98** 220407(R)
[16] Lee S H, Kikuchi H, Qiu Y, Lake B, Huang Q, Habicht K and Kiefer K 2007 *Nat. Mater.* **6** 853
[17] Rao X, Hussain G, Huang Q, Chu W J, Li N, Zhao X, Dun Z, Choi E S, Asaba T, Chen L, Li L, Yue X Y, Wang N N, Cheng J-G, Gao Y H, Shen Y, Zhao J, Chen G, Zhou H D and Sun X F 2021 *Nat. Commun.* **12** 4949
[18] Ma Z, Wang J, Dong Z Y, Zhang J, Li S, Zheng S H, Yu Y, Wang W, Che L, Ran K, Bao S, Cai Z, Čermák P, Schneidewind A, Yano S, Gardner J S, Lu X, Yu S L, Liu J M, Li S, Li J X and Wen J 2018 *Phys. Rev. Lett.* **120** 087201
[19] Huang Z, Xu Z, Li S, Duan Q, Liao J, Bao S, Shangguan Y, Zhang B, Xu H, Cheng S, Song Z, Dong S, Wu M, Stone M B, Qiu Y, Zhong R, Xu G, Ma Z, Gu G D, Tranquada J M and Wen J 2025 *Phys. Rev. B* **112** 035128
[20] Ma Z, Chen Y, Fu Z, Li S, Tong X-A, Du H, Embs J P, Zheng S, Zhang Y, Liu M, Zhong R, Liu J-M and Wen J 2025 *Phys. Rev. B* **111** 155141
[21] Woodward P M, Sleight A W, Du L-Sh and Grey C P 1999 *J. Solid State Chem.* **147** 99
[22] Nalbandyan V B, Shukaev I L, Raganyan G V, Svyazhin A, Vasiliev A N and Zvereva E A 2019 *Inorg. Chem.* **58** 5524

[23] Zvereva E A, Raganyan G V, Vasilchikova T M, Nalbandyan V B, Gafurov D A, Vavilova E L, Zakharov K V, Koo H J, Pomjakushin V Y, Susloparova A E, Kurbakov A I, Vasiliev A N and Whangbo M H 2020 *Phys. Rev. B* **102** 094433

[24] Kurbakov A I, Susloparova A E, Pomjakushin V Y, Skourski Y, Vavilova E L, Vasilchikova T M, Raganyan G V and Vasiliev A N 2022 *Phys. Rev. B* **105** 064416

[25] Xu X, Chen G, Ni D, Gui X, Xie W, Yao N and Cava R J 2023 *Phys. Rev. Materials* **7** 024407

[26] Yamashita M, Nakata N, Senshu Y, Nagata M, Yamamoto H M, Kato R, Shibauchi T and Matsuda Y 2010 *Science* **328** 1246

[27] Murayama H, Sato Y, Taniguchi T, Kurihara R, Xing X Z, Huang W, Kasahara S, Kasahara Y, Kimchi I, Yoshida M, Iwasa Y, Mizukami Y, Shibauchi T, Konczykowski M and Matsuda Y 2020 *Phys. Rev. Research* **2** 013099

[28] Li N, Huang Q, Yue X Y, Chu W J, Chen Q, Choi E S, Zhao X, Zhou H D and Sun X F 2020 *Nat. Commun.* **11** 4216

[29] Freedman D E, Han T H, Prodi A, Müller P, Huang Q-Z, Chen Yu-S, Webb S M, Lee Y S, McQueen T M and Nocera D G 2010 *J. Am. Chem. Soc.* **132** 16185

[30] Li N, Neumann R R, Guang S K, Huang Q, Liu J, Xia K, Yue X Y, Sun Y, Wang Y Y, Li Q J, Jiang Y, Fang J, Jiang Z, Zhao X, Mook A, Henk J, Mertig I, Zhou H D and Sun X F 2023 *Phys. Rev. B* **108** L140402

[31] J. A. Mydosh 1993 *Spin Glass: An Experimental Introduction* (Taylor and Francis, London)

[32] Mydosh J A 2015 *Rep. Prog. Phys.* **78** 052501

[33] Lhotel E, Paulsen C, de Réotier P D, Yaouanc A, Marin C and Vanishri S 2012 *Phys. Rev. B* **86** 020410(R)

[34] Svoboda P, Javorský P, Diviš M, Sechovský V, Honda F, Oomi G and Menovsky A A 2001 *Phys. Rev. B* **63** 212408

[35] Hemberger J, Hoinkis M, Klemm M, Sing M, Claessen R, Horn S and Loidl A 2005 *Phys. Rev. B* **72** 012420

[36] Janíček P, Drašar Č, Lošták P, Vejpravová J and Sechovský V 2008 *Physica B* **403** 3553

[37] Wenger L E and Keesom P H 1976 *Phys. Rev. B* **13** 4053

[38] Nagata S, Galazka R R, Mullin D P, Akbarzadeh H, Khattak G D, Furdyna J K and Keesom P H 1980 *Phys. Rev. B* **22** 3331

[39] Galazka R R, Nagata S and Keesom P H 1980 *Phys. Rev. B* **22** 3344

[40] Huang C Y 1985 *J. Magn. Magn. Mater.* **52** 1

[41] Berman R 1976 *Thermal Conduction in Solids*, (Oxford University Press, Oxford)

[42] Zhao Z Y, Wang X M, Fan C, Tao W, Liu X G, Ke W P, Zhang F B, Zhao X and Sun X F 2011 *Phys. Rev. B* **83** 014414

[43] Tari A 2003 *Specific Heat of Matter at Low Temperatures* (Imperial College Press)

[44] Sun X F and Ando Y 2009 *Phys. Rev. B* **79** 176501

[45] Xu X, Chen J and Li B 2016 *J. Phys.: Condens. Matt.* **28** 483001

[46] Chen Z and Dames C 2015 *Appl. Phys. Lett.* **107** 193104

[47] Li H, Zheng W and Koh Y K 2018 *Phys. Rev. Materials* **2** 123802

[48] Li N, Brassington A, Shu M F, Wang Y Y, Liang H, Li Q J, Zhao X, Baker P J, Kikuchi H, Masuda T, Duan G, Liu C, Wang H, Xie W, Zhong R, Ma J, Yu R, Zhou H D and Sun X F 2024 arXiv:2405.13628

[49] Li N, Rutherford A, Wang Y Y, Liang H, Li Q J, Zhang Z J, Wang H, Xie W, Zhou H D and Sun X F 2024 *Phys. Rev. B* **110** 134401

[50] Arzoumanian C, De Goër A M, Salce B and Holtzberg F 1983 *J. Physique* **44** L39

[51] Li N, Xie M T, Huang Q, Zhuo Z W, Zhang Z, Choi E S, Wang Y Y, Liang H, Sun Y, Wu D D, Li Q J, Zhou H D, Chen G, Zhao X, Zhang Q M and Sun X F 2024 *Phys. Rev. B* **110** 224414

[52] Guang S K, Li N, Luo R L, Huang Q, Wang Y Y, Yue X Y, Xia K, Li Q J, Zhao X, Chen G, Zhou H D and Sun X F 2023 *Phys. Rev. B* **107** 184423

[53] Zhao X, Zhao Z Y, Chen L M, Rao X, Che H L, Chu L G, Zhou H D, Ling L S, Wang J F and Sun X F 2019 *Phys. Rev. B* **99** 104419

[54] Wang X M, Fan C, Zhao Z Y, Tao W, Liu X G, Ke W P, Zhao X and Sun X F 2010 *Phys. Rev. B* **82** 094405

[55] Li Q J, Zhao Z Y, Zhou H D, Ke W P, Wang X M, Fan C, Liu X G, Chen L M, Zhao X and Sun X F 2012 *Phys. Rev. B* **85** 174438

[56] Sun X F, Taskin A A, Zhao X, Lavrov A N and Ando Y 2008 *Phys. Rev. B* **77** 054436

[57] Sun X F, Tsukada I, Suzuki T, Komiya S and Ando Y 2005 *Phys. Rev. B* **72** 104501

[58] Suetsugu S, Ukai Y, Shimomura M, Kamimura M, Asaba T, Kasahara Y, Kurita N, Tanaka H, Shibauchi T, Nasu J, Motome Y, and Matsuda Y 2022 *J. Phys. Soc. Jpn.* **91** 124703

[59] Herlach D M, Wassermann E F and Willnecker R 1983 *Phys. Rev. Lett.* **50** 529

[60] Wassermann E F and Herlach D M 1984 *J. Appl. Phys.* **55** 1709